Electron Spin Double Resonance Studies of F Centers in KCl. I*

P. R. MORAN†
Laboratory of Atomic and Solid State Physics, Cornell University, Ithaca, New York
(Received 20 November 1963; revised manuscript received 9 March 1964)

This paper describes the investigation of the F-center electron-spin-resonance spectrum in KCl at 300°K using a double-frequency (DESR) technique. The inhomogeneously broadened resonance is saturated by an applied rf pump field and the spectrum is simultaneously probed by a weak detector field applied at a different frequency. The F-center concentrations in the samples studied were $n_F \lesssim 3\times10^{17}$ cm^{-3}. The techniques used in obtaining the experimental data are discussed and a theoretical treatment of the response of the spin system to two simultaneously applied fields is developed. The T_1-T_2 spin-packet model of the F-center resonance is specifically treated and a comparison of the experimental data with the theoretically predicted results indicates that this model, which has formed the basis of previous treatment, cannot be used in a consistent interpretation of the resonance properties of the KCl F-center system. A general expression is derived which relates the DESR signal area to the absorption intensity in a corresponding ESR experiment. The application of this relation to the data obtained in the experiments gives a KCl F-center spin-lattice relaxation time at 300°K of $T_1=0.3\times10^{-4}$ sec with an estimated uncertainty of 15%. A phenomenon which has not been previously considered in relation to the F-center absorption is observed in the existence of significant contributions to the absorption intensity from "forbidden" transition processes. These processes are attributed to a simultaneous electron and nuclear spin flip via the anisotropic terms in the hyperfine interaction. The large intensity associated with certain of these forbidden transitions is shown to imply a sufficiently rapid *nuclear* relaxation rate that the inhomogeneous broadening interactions may *not* be validly treated as a static phenomenon.

I. INTRODUCTION

THIS paper describes a double electron-spin-resonance technique (DESR) in which an inhomogeneously broadened spin system may be studied by the application of two independent rf fields. With the DESR technique one is able to investigate various mechanisms and interactions which may be responsible in determining certain aspects of the resonance behavior and which may remain obscure in the study of the conventional single-frequency (ESR) results. For example, the ESR spectrum of F centers in KCl has been pictured as being composed of a large number of individual "spin packets" which are distributed over a range in resonant frequencies due to the hyperfine interaction of the F-center electron with nearby potassium and chlorine nuclei. In this distribution the component multiplets, or spin packets, remain unresolved so that the observed ESR line shape is determined entirely by the inhomogeneous broadening process. One cannot, therefore, obtain direct information concerning the line shape or linewidth of the individual spin packets in the usual steady-state ESR experiment.

This model, in which one assumes that the ESR behavior of the F-center spin system can be satisfactorily described by a static inhomogeneous distribution of independent individual spin packets parameterized by a packet width $1/T_2$, and a spin-lattice relaxation rate $1/T_1$, is subsequently referred to in this paper as the T_1-T_2 model.

The specific interest in the F-center ESR system arises from previous experiments carried out at this laboratory[1] in which it was found that the dependence of the ESR absorption signal, $H_1\chi''$, upon the applied field strength, H_1, deviates from the behavior which had been expected. For the F-center spin-resonance model originally proposed by Portis,[2] $H_1\chi''$ is predicted to be independent of H_1 for sufficiently large H_1 and this behavior was experimentally verified over the range of H_1 then available. However, the results obtained here with higher power klystrons and independently by Gross and Wolf[3] indicate a "drooping" behavior for very large H_1 where the signal decreases from its maximum value as is shown in Fig. 1. In the Portis model one assumes that the spin packets have a Lorentzian shape and that their width is very small compared with the width of the inhomogeneous distribution. The experimentally observed dependence of the absorption signal upon H_1 which was shown in Fig. 1 could be qualitatively explained either if the packets were not narrow compared with the inhomogeneous breadth or if the wings of the packet shape were cut off more rapidly than those of a Lorentzian curve. The former case was treated by Castner[4] for experiments on the ESR spectrum of V_k centers and the latter case has been examined by Noble and Markham.[5]

Since, as was pointed out previously, conventional

* This paper is based upon the author's Ph.D. thesis completed under a National Science Foundation Predoctoral Fellowship at Cornell University. The research was partially supported by the U. S. Atomic Energy Commission.

† The author is presently a National Science Foundation Post-doctoral Fellow at the Physics Department, University of Illinois, Urbana, Illinois.

[1] P. R. Moran, S. H. Christensen, and R. H. Silsbee, Phys. Rev. **124**, 442 (1961).
[2] A. M. Portis, Phys. Rev. **91**, 1071 (1953).
[3] H. C. Wolf and H. Gross, Naturwiss. **8**, 299 (1961).
[4] T. G. Castner, Phys. Rev. **115**, 1506 (1959).
[5] J. J. Markham and G. A. Noble, Technical Report of the Armour Research Foundation of the Illinois Institute of Technology, ARF 1184-2 (unpublished).

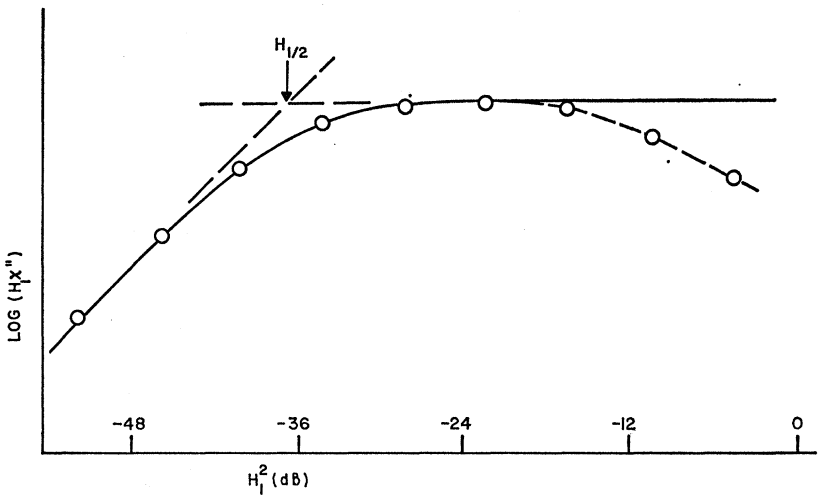

FIG. 1. ESR absorption signal for KCl F centers at 300°K plotted as a function of applied field strength. The solid line shows the behavior predicted in the limit of infinite homogeneous width for Portis' spin packet model. The circles are experimental points.

ESR experiments on this inhomogeneously broadened system provide no direct information concerning the packet width or shape, other techniques must be employed in order to study these properties. One such technique is to "eat a hole" in the line by applying a heavily saturating field at a particular frequency. Figure 2 illustrates how the packets with resonant frequencies near the applied frequency are more heavily saturated than those whose resonant frequencies are farther from the applied frequency. The dotted curve in Fig. 2 represents the signal one would observe if the saturating field were reduced and swept through the line before spin-lattice processes could restore thermal equilibrium. The shape of the "hole" is closely related to the shape of the packets and transient techniques as described above have been used to study the F-center system at liquid-helium temperatures by Noble[6] and more recently by Seidel[7] up to liquid-nitrogen temperature.

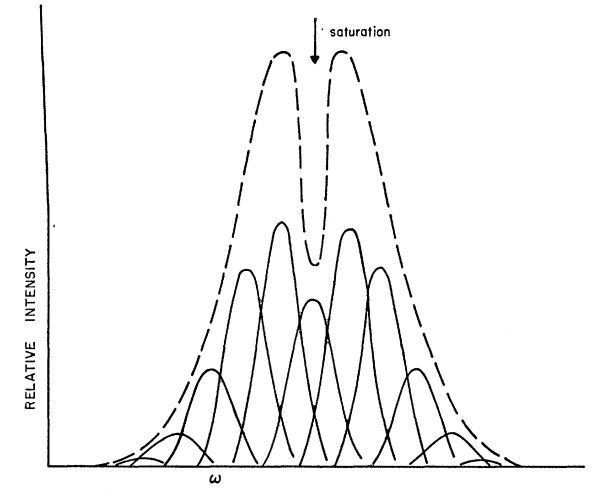

FIG. 2. Saturation of an inhomogeneous line. The rf field applied at the frequency $\omega_{\text{saturation}}$ tends to saturate most heavily those packets whose resonant frequencies are close to the applied frequency.

The DESR experiment discussed in this paper is a steady-state investigation in which one rf field (subsequently called the "pump" field) is applied to the line at a frequency ω_p as indicated in Fig. 3. The hole which this pump field burns in the line is simultaneously probed by a weak second rf field (subsequently called the "detector" field) at a frequency ω_d. The resulting detector signal can be analyzed to determine the steady-state hole shape produced by the saturation of longitudinal magnetization in the spectral region about ω_p. In addition, as is shown in a later section, certain components of the detector signal may be interpreted as arising from the precessing transverse magnetization created by the pump fields and the behavior of these components can provide other information relating to processes which cause the decay of induced transverse magnetization.

II. THE DESR EXPERIMENT

Experimental Equipment

A block diagram of the apparatus used in the DESR experiment on KCl F centers is given in Fig. 4. The principal component parts are the detector system, the sample cavity, the pump system, and devices for measuring the frequency difference between the pump and detector klystrons.

The detector system. The detector arm of the apparatus is a conventional 3-cm microwave spectrometer using balanced bolometer detection[2] and employing a Varian V-58 klystron which is stabilized to a reference cavity. The lock-in detection system operated at 35 cps and

[6] G. A. Noble, Phys. Rev. 118, 1024 (1960).
[7] H. Seidel, 1962 International Symposium on Color Centers in Alkali Halides, Technischen Hochschule, Stuttgart (unpublished).

the modulation was achieved either by a square-wave chopping of the pump power with a ferrite modulator or by the standard technique of magnetic field modulation.

The pump system. The pump arm consists of a second Varian V-58 stabilized to a second reference cavity, a ferrite modulator when pump power modulation is desired, a calibrated attenuator, a slide screw tuner, and a dual directional coupler for monitoring incident and reflected power.

Difference frequency measurement. A small fraction of pump and detector powers were coupled into an isolated magic tee and mixed in a crystal mounted in a common arm from which the resulting difference frequency could be measured. Measurements on this difference frequency indicated a short term stability, given by the rf sideband spectrum of the difference signal, of about five kilocycles. Long term drift in the difference frequency could be seen on the monitoring equipment and corrected manually during the course of a run.

The sample cavity. The sample cavity operated in the cylindrical TM_{110} modes, the equivalent 90° rotations of which serve as orthogonal pump and detector modes. The front plate of the cavity, upon which the samples were mounted, is a choke flange appropriate to the frequency and mode symmetry employed and is used to eliminate the problem of high-resistivity joints. The pump and detector irises are placed as shown in Fig. 5 and the tuning screws shown in the figure enable one to set the frequency difference between the modes and to tune out any cross coupling between the pump and detector wave guides.

This requirement of no cross coupling between guides is a most important experimental consideration since the desired signal, which is present in the reflected detector power, can be 100 dB or more smaller than the amplitude of the pump fields present in the pump wave guide. Under these circumstances, if even a relatively small fraction of the pump power is coupled into the detector wave guide it may, because of imperfect bolometer matching, unbalance the detector bridge and tend to swamp the system's response to the actual DESR signal.

It was found that in order to preserve linearity of the detection system and to eliminate unwanted contributions from the spurious feed-through, it was necessary to have greater than 60 dB rejection between the two guides. This requirement is relatively easily met if the

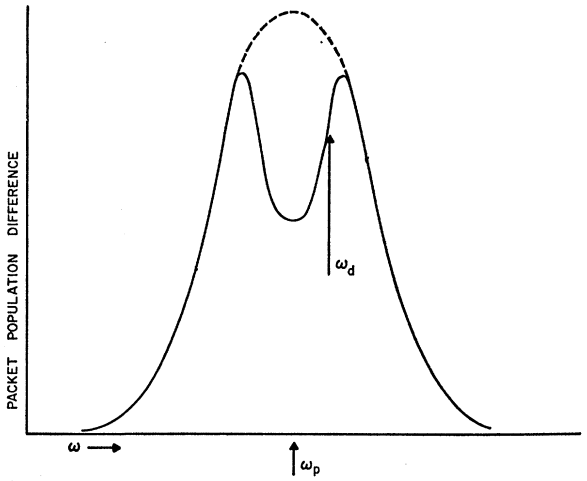

FIG. 3. The hole eaten in the inhomogeneous line by the pump field at a frequency ω_p is probed by a weak detector field at a frequency ω_d.

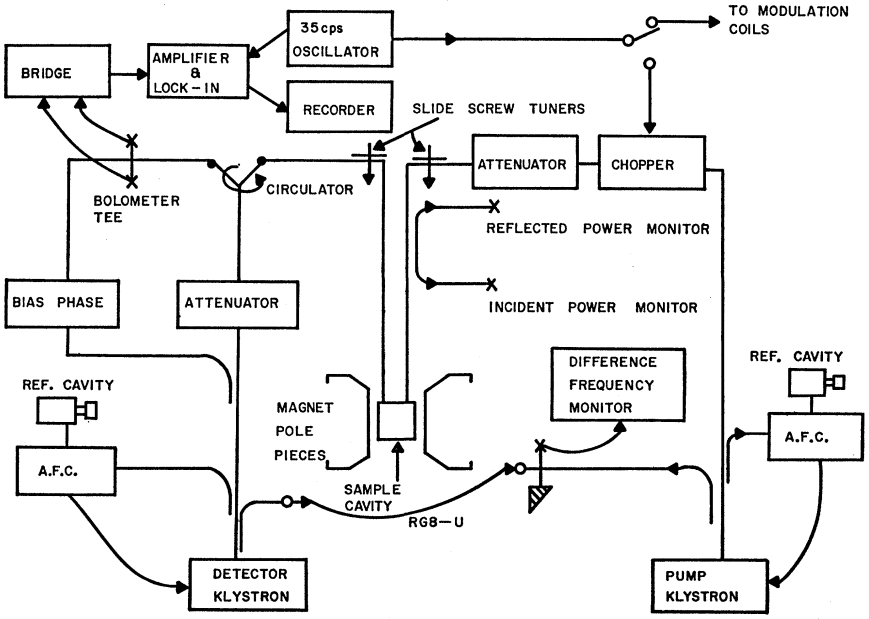

FIG. 4. Block diagram of the DESR spectrometer.

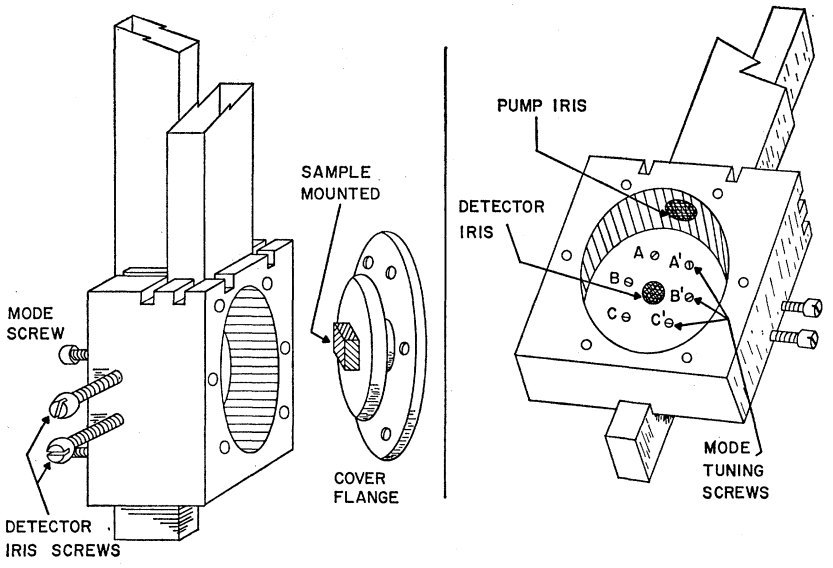

FIG. 5. The bimodal sample cavity. The tuning screws A—A′ and C—C′ are, respectively, the resistive and reactive mode rotation pairs. The tuning screws B and B′ are the mode splitting screws which are used to determine the mode frequency difference. The operation of these elements is discussed in the text.

two modes are separated by more than a few times their response width, but in the particular experiments described here it was necessary to have pump and detector modes essentially degenerate. Under these conditions one must provide means for tuning out both reactive and resistive couplings between the modes as well as a mechanism for adjusting the spatial coupling parameters of at least one of the irises. An extension of the techniques developed by Bethe and Schwinger[8] was used to calculate the types and positions of the tuning screws necessary to meet the requirements mentioned above. By following a careful tuning procedure guide-to-guide rejection, which is independent of frequency, can be made to exceed 80 dB (the limit of the sensitivity of the measuring equipment used) even when the modes are split by less than a few kilocycles.

Samples and Experimental Results

The KCl samples used in the experiment were of Harshaw material cleaved to about 7 mm square by 2 mm thick. These were additively colored to concentrations of roughly 3×10^{17} centers/cc using the coloring apparatus described by van Doorn.[9] Since the amplitude of the rf magnetic field is uniform along the axis of a cylindrical TM_{110} cavity, the signal-to-noise ratio could be improved with no sacrifice of rf field homogeneity by stacking several of the simultaneously prepared thin samples to obtain a final specimen of about 8 mm thickness. The samples were quenched from 700°C into a CCl_4 bath and were mounted in the cavity under low-level red illumination to insure a satisfactorily high F- to M-center ratio.

To begin an experimental run the cavity modes were set at a difference frequency appropriate to the range of the pump-detector klystron difference frequency Δ, which was desired and the cross coupling was tuned out. Since the convenience of being able to tune Δ over a relatively broad range without retuning the cavity justified a certain loss in signal-to-noise ratio some sources of loss had been incorporated into the cavity to give a relatively low Q, resulting in a cavity half-power half-width of about 5 Mc.

The detector klystron was run at a fixed frequency and the pump frequency was varied while the reflected pump power was monitored and the slide-screw tuner adjusted to maintain critical coupling to the cavity pump mode. With the detector bias phase set for sensitivity to the absorption component and the pump attenuator adjusted to the desired value, the frequency of the pump source reference cavity of the pump-arm a.f.c. system was varied in a point by point fashion over a range of about 4 Mc to trace out the DESR signal shape as a function of Δ.

In order that the data might be easily interpreted it was necessary to keep the detector field strength, $H_1(\text{detector})\equiv D$, sufficiently small that the system's response would be linear in D. This condition was found to be satisfactorily obtained as long as D was at least 3 dB smaller than $H_{1/2}$ although the data presented in this paper were taken with D more than 6 dB smaller than $H_{1/2}$.

The data presented in this paper are the steady-state

[8] The details of these calculations, which are based upon an extension of the methods of H. A. Bethe and J. Schwinger, N.R.D.C. Contractors Report D-1, No. 117 (PB-18340) (unpublished), and H. A. Bethe, M.I.T. Radiation Laboratory Report No. 194 (43-22) (unpublished) are given, along with a detailed description of the cavity tuning procedure, in the author's thesis (University Microfilms, Ann Arbor, Michigan). Treatments of similar problems using somewhat different methods have also been carried out by W. Lin [J. Appl. Phys. **22**, 989 (1951)], J. O. Artman and P. E. Tannenwald [J. Appl. Phys. **26**, 1124 (1955)], and A. M. Portis and D. Teaney [J. Appl. Phys. **29**, 1692 (1958)].

[9] C. Z. van Doorn, Rev. Sci. Instr. **32**, 775 (1961).

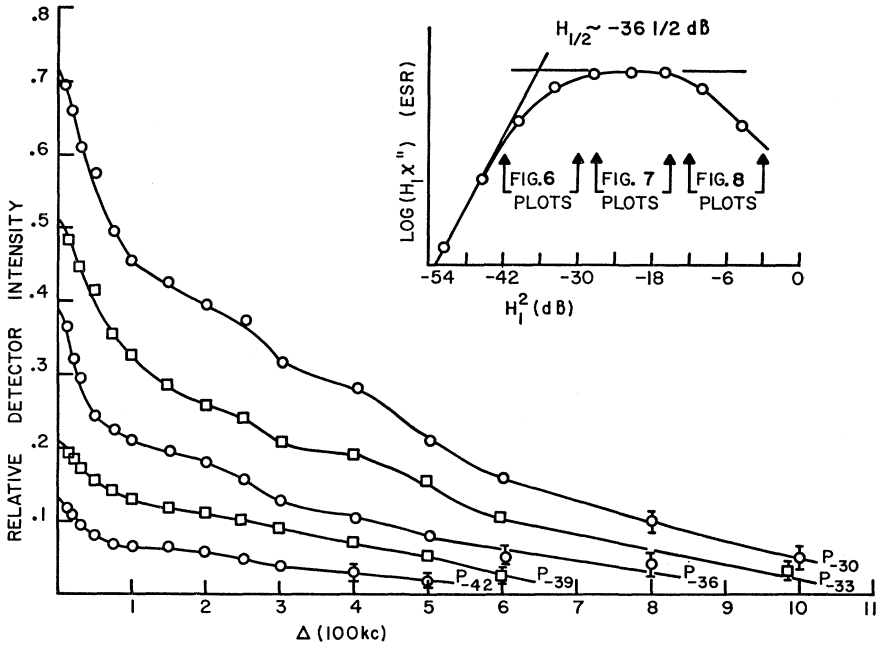

FIG. 6. DESR plots for KCl F centers with P from -42 dB to -30 dB. Zero dB is the maximum available pump power and corresponds to an applied field in the sample cavity of $P_{0dB} \approx 8.6 \times 10^6$ sec^{-1} or 0.49 G. The insert shows the corresponding ranges in the ESR saturation plot.

relative detector signal, $S(P,\Delta)$, which is defined as the difference between the detector field absorption signals with $H_1(\text{pump}) = P$ and $H_1(\text{pump}) = 0$ when the pump-detector frequency difference is Δ, divided by the detector field absorption signal with $H_1(\text{pump}) = 0$ when the pump-detector frequency difference is zero.

In subsequent sections of this paper the field levels expressed in decibels are referred to the maximum output power available at the cavity from the pump klystron. Experiments were performed on several samples all of which had roughly the same F-center concentration and the data presented below include runs on most of these different specimens.

Figure 6 shows the relative DESR signals with P ranging from about 6 dB below $H_{1/2}$ to about 6 dB above $H_{1/2}$. Figure 7 shows the DESR signal for P ranging from 9 dB above $H_{1/2}$ to about 21 dB above $H_{1/2}$. Figure 8 shows the DESR signals for pump levels where the conventional ESR saturation plots begin to "droop" from the Portis plot. These levels range from 24 dB above $H_{1/2}$ to 36 dB above which is the maximum pump power available and corresponds, therefore, to 0 dB on the field intensity scale used.

These figures show only half of the symmetric DESR signal although some of those presented are for Δ positive and some are for Δ negative.

III. DESR THEORETICAL APPROACH

Density Matrix Calculations

$T_1 - T_2$ model. Although a more general model is to be treated in a subsequent paper, it is instructive to begin with the $T_1 - T_2$ picture of Bloch.[10] In this model one supposes that the spin system is placed in a static magnetic field whose direction defines the z axis of a Cartesian coordinate system. It is assumed that the effects of spin-lattice interactions can be described in terms of a relaxation process which tends to restore the net longitudinal magnetization M_z to its thermal-equilibrium value at an average rate ω_1. This rate is the inverse of the characteristic spin-lattice time T_1 and

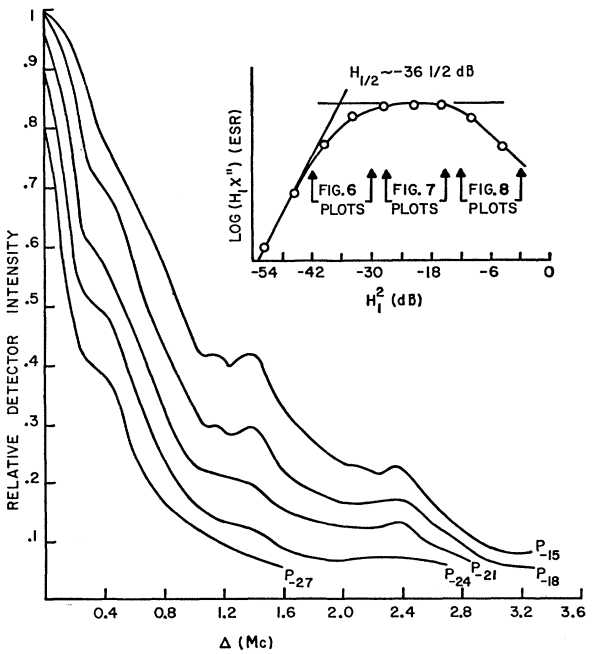

FIG. 7. DESR plots for KCl F centers with P from -27 to -15 dB (see Fig. 6).

[10] F. Bloch, Phys. Rev. **70**, 460 (1946).

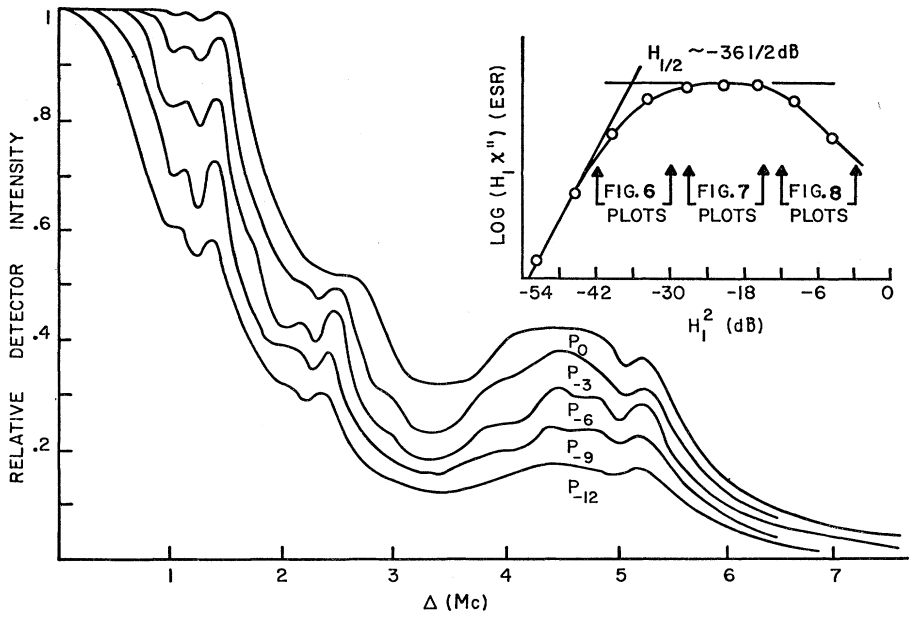

FIG. 8. DESR plots for KCl F centers with P from -12 to 0 dB (see Fig. 6).

it is assumed that ω_1 is independent of the other parameters which describe the experiment. Similarly one assumes a relaxation rate ω_2 for the transverse components of magnetization M_x and M_y. This transverse relaxation rate is the inverse of the characteristic "dephasing" time T_2 and may be larger than ω_1.

Under these assumptions the equations of motion for the density matrix, ρ, of the spin system[11] may be written in the form

$$\partial\rho/\partial t=-i[\mathcal{H},\rho]-\omega_{1,2}(\rho-\rho_0)\,, \tag{3.1}$$

where $\omega_{1,2}$ means that ω_1 is to be used for the diagonal terms of ρ, i.e., those corresponding to M_z, and ω_2 is to be used for the off-diagonal terms which correspond to the transverse components, $M_x\pm iM_y$. In Eq. (3.1) the Hamiltonian term in the commutator brackets has units of sec^{-1} ($\hbar=1$) and contains all the pertinent spin-system interactions with the exception of those which are accounted for in the relaxation terms.

The magnetic fields are also expressed in units of sec^{-1} and the conversion factor is

$$H(\text{sec}^{-1})=\gamma H(\text{gauss})\,, \tag{3.2}$$

where $\gamma=2\pi\times2.8\times10^6$ sec^{-1}/G for free electrons. The Hamiltonian term in Eq. (3.1) is therefore taken to be

$$\mathcal{H}=-H_0S_z-\mathbf{H}_{\text{rf}}(t)\cdot\mathbf{S}\,, \tag{3.3}$$

where H_0 is the strength of the applied static field, $\mathbf{H}_{\text{rf}}$ is the strength of the applied rf fields, and $\mathbf{S}$ is the usual spin operator for the case of spin-$\frac{1}{2}$ particles being considered here. The form of the thermal equilibrium density matrix ρ_0 is

$$\rho_0=\begin{pmatrix}1/2(1+M_0) & 0\\ 0 & 1/2(1-M_0)\end{pmatrix}, \tag{3.4}$$

where

$$M_0=\frac{n_+-n_-}{n_++n_-}\ \text{(thermal equilibrium)}\,, \tag{3.5}$$

$$n_+=\text{number of spins with } M_z=+\tfrac{1}{2}\,, \tag{3.6a}$$

$$n_-=\text{number of spins with } M_z=-\tfrac{1}{2}\,. \tag{3.6b}$$

By taking ρ_0 to be of the form given in Eq. (3.4) it has been implicitly assumed that the spin system relaxes along the direction of H_0 rather than along the instantaneous field direction. This is a valid approximation since $\mathbf{H}_{\text{rf}}(t)$ is many orders of magnitude smaller than H_0.

Those components of the linearly polarized rf magnetic fields which rotate in the anti-Larmor sense are neglected and the resulting Hamiltonian of Eq. (3.3) is

$$\mathcal{H}=-H_0S_z+\tfrac{1}{2}iP(S_+e^{ipt}-S_-e^{-ipt})+\tfrac{1}{2}iD(S_+e^{idt}-S_-e^{-idt})\,, \tag{3.7}$$

where p and d are the angular frequencies of the pump and detector fields respectively. It is convenient to transform the equations to a frame[12] which is rotating with the pump field $P(t)$, in which the transformed Hamiltonian is

$$\mathcal{H}_{\text{rot}}=-HS_z+\tfrac{1}{2}iP(S_+-S_-)+\tfrac{1}{2}i(S_+e^{i\Delta t}-S_-e^{-i\Delta t})\,, \tag{3.8}$$

[11] A. Abragam, *The Principles of Nuclear Magnetism* (Oxford University Press, New York, 1961). See Chap. II for an introduction to the density matrix equations for a two-level system.

[12] I. I. Rabi, N. F. Ramsey, and J. Schwinger, Rev. Mod. Phys. **26**, 167 (1954).

where

$$H=(H_0-p), \tag{3.9}$$

and

$$\Delta=(d-p). \tag{3.10}$$

The detector amplitude, D, is assumed small and treated as a perturbation so that by taking ρ to be of the form

$$\rho=\rho_0+\begin{pmatrix}\alpha & \gamma\\ \gamma^* & -\alpha\end{pmatrix}+\begin{pmatrix}\beta & \delta\\ \delta^* & -\beta\end{pmatrix}, \tag{3.11}$$

with the β and δ terms of order D, the approximate equations of motion are

$$\partial\alpha/\partial t=-\tfrac{1}{2}P(\gamma+\gamma^*)-\omega_1\alpha, \tag{3.12a}$$

$$\partial\gamma/\partial t=iH\gamma+P(\tfrac{1}{2}M_0+\alpha)-\omega_2\gamma, \tag{3.12b}$$

$$\partial\beta/\partial t=\tfrac{1}{2}P(\delta+\delta^*)+\tfrac{1}{2}D(\gamma e^{-i\Delta t}+\gamma^* e^{i\Delta t})-\omega_1\beta, \tag{3.13a}$$

and

$$\partial\delta/\partial t=iH\delta-P\beta-D(\tfrac{1}{2}M_0+\alpha)e^{i\Delta t}-\omega_2\delta, \tag{3.13b}$$

where the thermal-equilibrium term ρ_0 is expressed in the form given in Eq. (3.4).

Calculation of the absorbed power. The power absorbed from the rf fields $D(t)$ and $P(t)$ may be calculated by finding the expectation value of the operators $(\mathbf{M}\cdot d\mathbf{D}(t)/dt)$ and $(\mathbf{M}\cdot d\mathbf{P}(t)/dt)$. The operator $(\mathbf{M}\cdot d\mathbf{D}(t)/dt)$, for example, is expressed in matrix form as

$$(\mathbf{M}\cdot d\mathbf{D}(t)/dt)=-\tfrac{1}{2}dD\begin{pmatrix}0 & e^{i\Delta t}\\ e^{-i\Delta t} & 0\end{pmatrix}, \tag{3.14}$$

in the rotating frame. The power absorption expectation value is found from the trace of the matrix product of the density matrix with the absorption operators. The detector absorption, for example, is obtained, using Eqs. (3.14) and (3.11), as

$$\mathrm{Tr}[\rho(\mathbf{M}\cdot d\mathbf{D}(t)/dt)]=\tfrac{1}{2}dD[(\gamma+\delta)e^{-i\Delta t}+\text{c.c.}], \tag{3.15}$$

It can be seen from the form of Eq. (3.15) that only those terms in $(\gamma+\delta)$ which have an $\exp(i\Delta t)$ time dependence will contribute to the signal in a dc absorption measurement.

The steady-state solution for the first order, i.e., δ and β, terms are found to have only a dc and an $\exp(\pm i\Delta t)$ time dependence so that $\delta(t)$ may be written

$$\delta(t)=\delta_+e^{i\Delta t}+\delta_0+\delta_-e^{-i\Delta t}, \tag{3.16}$$

and $\beta(t)$ as

$$\beta(t)=\beta_+e^{i\Delta t}+\beta_0+\beta_-e^{-i\Delta t}, \tag{3.17}$$

where, since β is real, $\beta_+=\beta_-^*$.

To determine the dc detector absorption from the relation given in Eq. (3.15), one need only find the δ_+ term (γ has no steady-state time dependence). This is found to contain three distinct contributions so that δ_+ may be expressed as

$$\delta_+=\delta_{+\frac{1}{2}M_0}+\delta_{+\alpha}+\delta_{+\beta}, \tag{3.18}$$

where

$$\delta_{+\frac{1}{2}M_0}=-D\tfrac{1}{2}M_0[\omega_2+i(\Delta-H)]^{-1}, \tag{3.19a}$$

$$\delta_{+\alpha}=-D\alpha[\omega_2+i(\Delta-H)]^{-1}, \tag{3.19b}$$

and

$$\delta_{+\beta}=-P\beta_+[\omega_2+i(\Delta-H)]^{-1}. \tag{3.19c}$$

The thermal equilibrium magnetization M_0 is obtained from Eq. (3.5a), the pump induced longitudinal magnetization α from the solution of Eqs. (3.12a) and (3.12b), the β_+ term is obtained from a straightforward, although tedious, solution[13] of Eqs. (3.12a) and (3.12b) in which one finds

$$\beta_+=\frac{-\tfrac{1}{2}DP(\tfrac{1}{2}M_0)(\omega_2^2+H^2)[\omega_2+i(\Delta+H)](2\omega_2+i\Delta)}{(\omega_2+iH)[\omega_2^2+P^2(\omega_2/\omega_1)+H^2]\{[(\omega_2+i\Delta)^2+H^2](\omega_1+i\Delta)+P^2(\omega_2+i\Delta)\}}. \tag{3.20}$$

Thus the detector power absorbed, W_D, is found from Eq. (3.15) to be

$$W_D=dD\Re(\delta_{+\frac{1}{2}M_0}+\delta_{+\alpha}+\delta_{+\beta}), \tag{3.21}$$

where this absorption is that due to a particular group of spins, i.e., one "packet," all of which have the same effective z component of field H in the rotating frame. In order to find the total detector absorption, $W_{D(\text{total})}$, one may integrate the expression given in Eq. (3.21) over the appropriate inhomogeneous distribution of H;

$$W_{D(\text{total})}=dD\Re\int(\delta_{+\frac{1}{2}M_0}+\delta_{+\alpha}+\delta_{+\beta})dH. \tag{3.22}$$

If it is assumed that the inhomogeneous width, $1/T_2^*$, is very much greater than ω_2 and that the pump frequency is centered on the inhomogeneous line, then the three integrals in Eq. (3.22) can be computed by standard contour integration methods.

Discussion of the detector absorption terms. Under the assumptions mentioned in the preceding paragraph, which are found to be valid for the experiment described in this paper, the first integral on the right-hand side of Eq. (3.22) is calculated, using Eq. (3.19a), to obtain

$$dD\Re\int\delta_{+\frac{1}{2}M_0}dH=-dD^2\tfrac{1}{2}M_0\pi. \tag{3.23}$$

Note that this is just the total detector absorption, for small D, $W_D(P,\Delta)_{(\text{total})}$, for the special case of $P=0$ where one now has $\frac{1}{2}M_0$ defined as the thermal equilibrium magnetization per unit frequency.

[13] W. A. Anderson, Phys. Rev. **102**, 151 (1956). Analogous solutions obtained from the Bloch equations are presented in this paper for a double nuclear-magnetic-resonance experiment.

The second integral on the right of Eq. (3.22) is

$$dD\mathcal{R}\int\delta_{+\alpha}dH=dD^2\tfrac{1}{2}M_0\pi\left\{\frac{P^2(\omega_2/\omega_1)}{[\omega_2^2+P^2(\omega_2/\omega_1)]^{1/2}[\omega_2+(\omega_2^2+P^2\omega_2/\omega_1)^{1/2}]}\right\}\left\{1+\left[\frac{\Delta}{\omega_2+(\omega_2^2+P^2\omega_2/\omega_1)^{1/2}}\right]^2\right\}^{-1}. \quad (3.24)$$

This contribution to $W_D(P,\Delta)_{(\text{total})}$ is subsequently called the "hole contribution" since the first two terms on the right-hand side of Eq. (3.24) may be interpreted as the depth of the hole eaten by the pump field while the last term may be interpreted as the observed shape of a hole of width $[\omega_2^2+P^2(\omega_2/\omega_1)]$ folded with a detector resolution of ω_2.

The last integral on the right side of Eq. (3.22) involves the $\delta_{+\beta}$ term and it is found that this contribution to $W_{D(\text{total})}$ comes from the precessing induced transverse magnetization interacting with the detector field. It is an analogous term which, in the case of homogeneous NMR lines, gives rise to the phenomenon of "rotary saturation" treated by Redfield.[14] The DESR signal due to the $\delta_{+\beta}$ term is therefore subsequently referred to as the "rotary saturation" component.

Two features of the rotary saturation contribution to the detector absorption are of particular importance. First, consider the behavior of $\delta_{+\beta}$ as determined from the relations in Eqs. (3.19c) and (3.20). Note that, in the limit of heavily saturating P, the $\delta_{+\beta}$ term decreases as P^{-2}. On the other hand, one finds that the $\delta_{+\alpha}$ contribution has a maximum amplitude which is independent of P in the limit of heavily saturating P. Therefore, one may neglect the contribution of the rotary saturation signal in comparison with the hole signal under the conditions of heavily saturating pump fields.

The second important feature may be seen by noting in Eqs. (3.19c) and (3.20) that $\delta_{+\beta}(P,\Delta)$ has a dependence upon Δ such that the only poles of the function with respect to Δ are in the positive imaginary half-plane. Therefore, the integral over Δ of the rotary saturation signal must be zero. That is, the rotary saturation signal contribution to $W_D(P,\Delta)_{(\text{total})}$ is a contribution with zero net area under its curve as a function of Δ. In Appendix I it is shown that this is a general relation which does not depend upon the model chosen to describe the spin system response.

For weakly saturating pump fields, where the rotary saturation term may be comparable to the hole term, the third integral on the right of Eq. (3.22) is

$$dD\mathcal{R}\int\delta_{+\beta}dH$$
$$=dD^2\tfrac{1}{2}M_0\pi(P^2/2\omega_2\omega_1)[1-(\Delta^2/2\omega_2\omega_1)]$$
$$\times[1+(\Delta/\omega_1)^2]^{-1}[1+(\Delta/2\omega_2)^2]^{-1}, \quad (3.25)$$

which is symmetric in Δ and, as previously noted, has zero area as a function of Δ.

The relative DESR signal. The spectrometer signal which is studied in this experiment is the relative detector signal, $S(P,\Delta)$, which is defined as

$$S(P,\Delta)=\frac{W_D(P,\Delta)_{(\text{total})}-W_D(0,\Delta)_{(\text{total})}}{W_D(0,0)_{(\text{total})}}. \quad (3.26)$$

These relative DESR signals are experimentally determined by the procedure discussed in Sec. II of this paper and plots of $S(P,\Delta)$ for KCl F centers at room temperature are given in Figs. 8–10.

From Eqs. (3.22) and (3.23) one may obtain

$$S(P,\Delta)=\frac{\int\delta_{+\alpha}(P,\Delta,H)dH+\int\delta_{+\beta}(P,\Delta,H)dH}{\int\delta_{+\frac{1}{2}M_0}(P,0,H)dH} \quad (3.27)$$

and for the T_1-T_2 model, in the limit $P^2\ll\omega_1\omega_2$, i.e., weakly saturating pump, this is found to be

$$S(P,\Delta)=(P^2/2\omega_2\omega_1)\{[1+(\Delta/2\omega_2)^2]^{-1}+[1-(\Delta^2/2\omega_2\omega_1)]$$
$$\times[1+(\Delta/2\omega_2)^2]^{-1}[1+(\Delta/\omega_1)^2]^{-1}\}. \quad (3.28)$$

Figure 9 illustrates $S(P,\Delta)$ as obtained from Eq. (3.28) for the cases $\omega_1=0.1\ \omega_2$ and $\omega_1=\omega_2$. When $\omega_1\ll\omega_2$ the relative DESR signal may be approximately described as a Lorentzian spike of height $(P^2/2\omega_1\omega_2)$ with half-width ω_1 superimposed on a broad Lorentzian pedestal of height $(P^2/2\omega_1\omega_2)$ and half-width $2\omega_2$. For the case $\omega_1=\omega_2$, one finds that the hole, i.e., $\delta_{+\alpha}$, and the rotary saturation, i.e., $\delta_{+\beta}$, contributions have combined to produce a simple Lorentzian DESR signal with a height (P^2/ω_1^2) and half-width ω_1.

Comparison with experiment. The relative DESR signal predicted for the T_1-T_2 model, and given in Eq. (3.28) for $P^2\ll\omega_1\omega_2$, can be compared with the experimentally determined $S(P,\Delta)$ for the case of weakly saturating pump fields. In Fig. 10 the experimental points were taken for $P=-42$ dB and the theoretical curve was obtained by choosing $\omega_1=2\pi\times2\times10^4$ sec^{-1}, $\omega_2=2\pi\times1.75\times10^5$ sec^{-1}, and $P^2=2.2\times10^{10}$ sec^{-2}.

Although Fig. 10 seems at first to indicate fair qualitative agreement between the experimental results and the predictions of the T_1-T_2 model, the parameters derived by forcing this agreement require an assumed value of P^2 which is about a factor of 5 larger than the

[14] A. G. Redfield, Phys. Rev. **98**, 1787 (1955).

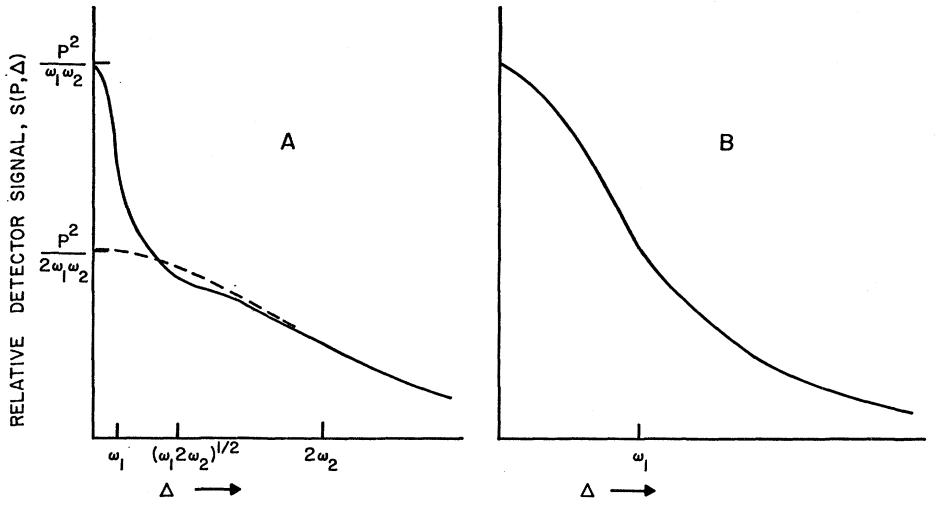

FIG. 9. DESR signals predicted for the T_1-T_2 model in the limit of weakly saturating pump fields. Diagram (A) shows the signal for $\omega_1 \approx 0.1\ \omega_2$ and (B) shows the signal for the case $\omega_1=\omega_2$.

actual experimental value. This discrepancy is closely related to the fact that the $\omega_1\omega_2$ product necessary to obtain the curve in Fig. 10 is a factor of 5 larger than the value of $H_{1/2}^2$ measured in an ESR saturation experiment. These inconsistencies are of a very basic nature because they are observed at weakly saturating pump field levels where the numbers which one derives are not critically dependent upon the details of the assumed packet shape and where there is negligible contribution to the absorption from the structure observed at higher rf levels.

In view of these observations, it is not surprising that one finds that DESR signals observed at higher pump levels also cannot be interpreted in terms of the T_1-T_2 model even though this model can be extended, as indicated later, to account for the "forbidden transition" structure.

It is evident from the above comparisons that the Lorentzian shape T_1-T_2 model (or any static-spin-packet model) cannot account for the KCl F-center DESR response observed in this experiment.

The Area Under DESR Signals

Although the specific details of the predicted DESR signal depend upon the particular model chosen to represent the spin system's response it is possible to derive a general relation concerning the area under the DESR curve which is independent of the model and which can provide useful information about certain aspects of the system's behavior. This relation is derived in Appendix I and may be expressed in the form

$$(\tfrac{1}{2}M_0)\omega_1\int_{-\infty}^{\infty} S(P,\Delta)d\Delta/P=P\chi''(\text{pump};P). \quad (3.29)$$

The quantity $(\frac{1}{2}M_0)$ may be experimentally determined since, for pump fields which are sufficiently small to be in the range of linear response of the system, it can be easily shown that

$$P\chi''_{\text{unsaturated}}=P\tfrac{1}{2}M_0\pi. \quad (3.30)$$

Figure 11 compares the ESR saturation plot of $[P\chi''(\text{pump};P)]$ with the values of $\int_{-\infty}^{\infty} S(P,\Delta)d\Delta/P$ plotted as a function of P. The ordinate scales are normalized to give the best agreement in accordance with the relation in Eq. (3.31) and the value of this normalization factor is used to calculate ω_1:

$$\omega_1=(1/T_1)=3\times10^4\ \text{sec}^{-1}. \quad (3.31)$$

The estimated error in this room temperature value is about 15% which arises mostly from uncertainties in determining the value of P.

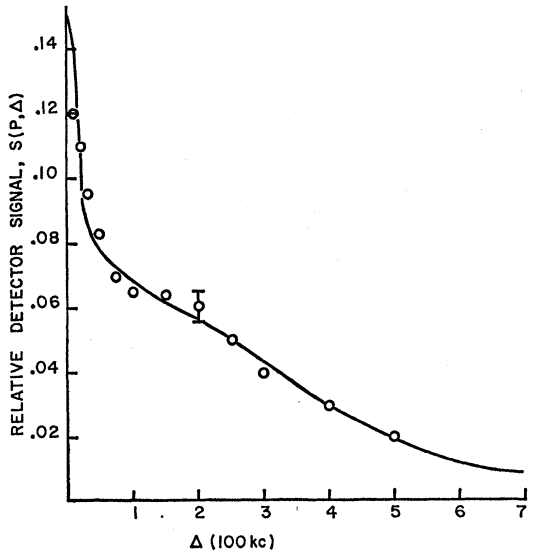

FIG. 10. DESR signals at low pump intensity. The circles are experimental points on KCl F centers for $P=-42$ dB and the solid line is a theoretical curve obtained from the T_1-T_2 model by taking $\omega_1=2\pi\times20$ kc, $\omega_2=2\pi\times175$ kc, and $P^2=2.2\times10^{10}$ sec^{-2}.

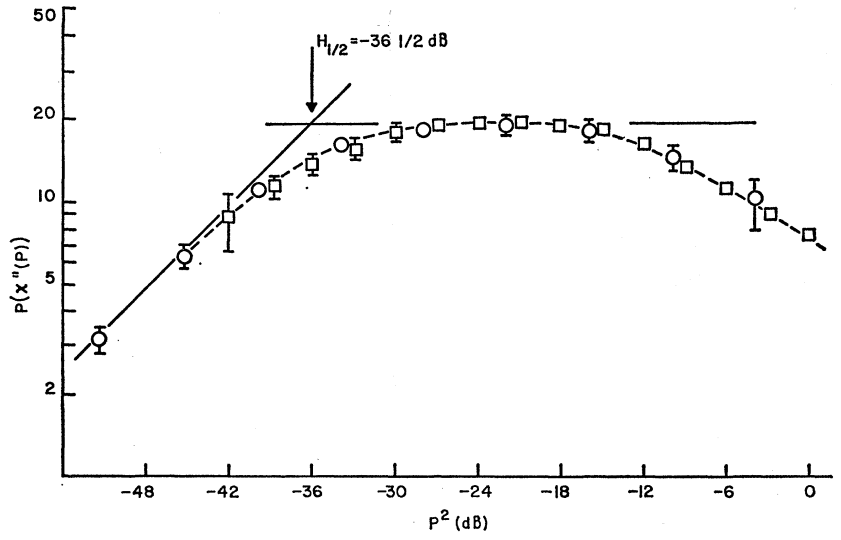

FIG. 11. ○, the single frequency ESR signal. □, the relative DESR signal, $S(P,\Delta)$, integrated over Δ, divided by P, and multiplied by a numerical factor for normalization to the ordinate scale of the ESR signals.

Another practical consequence of the result expressed in Eq. (3.29), which shows that the *area* under the DESR curve depends only on the pump absorption for that value of P, is that one may perform calculations using, for example, the simple T_1-T_2 model and then compute the area under Δ to obtain predicted results which do not depend on the details of the model used. This allows one to compare certain theoretical and experimental results without concern over the peculiarities which arise from a particular picture of the response mechanisms.

Forbidden Transitions

Figure 12 illustrates the relative DESR signal, $S(P,\Delta)$, for $P=-9$ dB. This figure points out one of the high-pump-level DESR features, the appearance of structure in the "hole" under steady-state conditions at room temperature. The nuclear Zeeman frequencies for the static field of 3330 G used in this experiment are indicated by arrows in Fig. 12 at 1.39 Mc for Cl^{35}, 1.16 Mc for Cl^{37}, and 0.663 Mc for K^{39}. The dashed line in Fig. 12 is an estimate of a smooth background which will fit onto the tails of the curve at large values of Δ. The shaded area indicated in the figure is an estimate of the area associated with the chlorine Zeeman-frequency bumps.

This structure is interpreted as saturation of the resonance line by "forbidden transitions" in which an F-center electron and a neighboring nucleus undergo a simultaneous spin flip. The selection rules for this

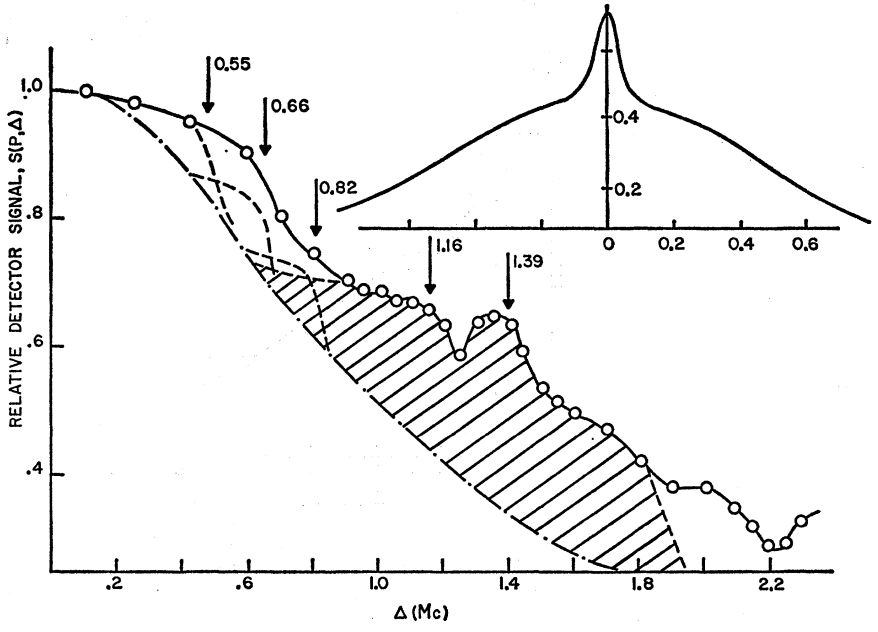

FIG. 12. ○, DESR signal, $S(P,\Delta)$, for $P=-9$ dB. The dashed lines and shaded area are discussed in the text. The insert shows $S(P,\Delta)$ for $P=-30$ dB with the ordinate drawn to one-half the scale of the main figure.

process are relaxed by the presence of anisotropic terms in the hyperfine coupling tensor and the resulting effect is the same as that observed in some narrow-line ESR spectra by Trammel, Zeldes, and Livingston.[15] This phonomenon has also been observed using transient techniques in low-temperature ESR studies of other inhomogeneous systems by Castle[16] and Feher and Gere.[17]

The expected intensities corresponding to such forbidden transitions are calculated in Appendix IIA where it is assumed that the *nuclear* relaxation times are sufficiently fast that there is no polarization of the nuclear system. If nuclear polarization was appreciable then, as shown in Appendix IIB, the forbidden transitions could not effectively maintain a steady-state saturation of the corresponding allowed transitions and no structure would be observed. It is found that those chlorine nuclei which are closer to the F center than shell VI, i.e., Cl sites in the (211) directions, have hyperfine couplings so large that the corresponding structure would not appear near the Zeeman frequency. Using the ENDOR data of Seidel,[18] Holton,[19] and Blumberg and Feher,[20] the total magnetization induced by forbidden transitions of Cl nuclei from the (2,1,1) and more distant sites is predicted (see Appendix IIA) to give an area under the *forbidden* transition structure for a pump level of -9 dB equal to one-half that under the *allowed* transition DESR signal at a pump level of -30 dB.

The insert in Fig. 12 shows the $P=-30$-dB DESR signal with the ordinate drawn to $\frac{1}{2}$ scale and, in spite of the uncertainties associated with the estimates of the background, etc., it can be seen that the two areas are, indeed, roughly equal. One may also note that the division in intensity between the maxima at 1.16 and and 1.39 Mc is consistent with the natural isotopic abundancy of the two chrlorine species.

The Cl nuclei of shell VI have a dominant contact hyperfine interaction with the F center of $(a/2)\approx 50$ kc. As is shown in Appendix IIB, the forbidden transition intensity in such a case is equally divided between the two components at 1.39+0.05 Mc and 1.39−0.05 Mc. The intensity of each of these components is shown in Appendix IIA to be just about equal to the intensity very close to 1.39 Mc due to all the Cl nuclei farther out than the shell-VI sites. One would, therefore, predict that the central maxima of the observed structure would exhibit a broad peak with a full width of about 100 kc as compared with the 40-kc width of the central maximum for the weakly saturated allowed-transition curve. The data in Fig. 12 shows that this

[15] G. T. Trammel, H. Zeldes, and R. Livingston, Phys. Rev. **110**, 630 (1958).
[16] J. Castle (private communication).
[17] G. Feher and E. A. Gere, Phys. Rev. **114**, 1245 (1959).
[18] H. Seidel, thesis, 2. Physikalisches Institut der Technischen Hochschule Stuttgart, 1961 (unpublished).
[19] W. C. Holton, thesis, University of Illinois, 1960 (unpublished).
[20] W. E. Blumberg and G. Feher, Bull. Am. Phys. Soc. **5**, 183 (1960).

TABLE I. Predicted difference frequencies for observing forbidden transitions.

Shell	No.	Ion	Direction		Δ_1 (Mc)	Δ_2 (Mc)
I	6	K^{39}	100	(ntdf)		
II	4	Cl^{35}	101		5.00	2.22
		Cl^{37}			4.17	1.87
	8	Cl	110	(ntdf)		
III	8	K	111		0.82	0.50
IV	6	Cl	200	(ntdf)		
V	12	K	201		0.66	0.66
	12	K	210	(ntdf)		
VI	8	Cl^{35}	211		1.46	1.32
		Cl^{37}			1.22	1.10
	16	Cl^{35}	121		1.43	1.35
		Cl^{37}			1.19	1.13

prediction is also in good agreement with the experimental results. One must conclude from these observations that the Cl forbidden transitions are playing a significant role in determining the ESR behavior and, in particular, that the 24 chlorine nuclei in shell VI contribute strongly to this effect.

It is tempting to associate the additional structure seen in Fig. 8 with nuclei closer to the F center than those of shell VI. Table I gives the expected Δ's for a number of nuclei as computed from ENDOR data.[18–02] The hyperfine coupling frequencies used in these calculations include both dipolar and contact terms and are calculated for H_0 parallel to the [100] direction which was the orientation used in this experiment. The nuclei having the notation "ntdf" in the table are those which, in this configuration, have "no transverse dipolar fields" and which, therefore, are not expected to contribute forbidden transitions.

In Fig. 13 the predicted Δ's from Table I correspond-

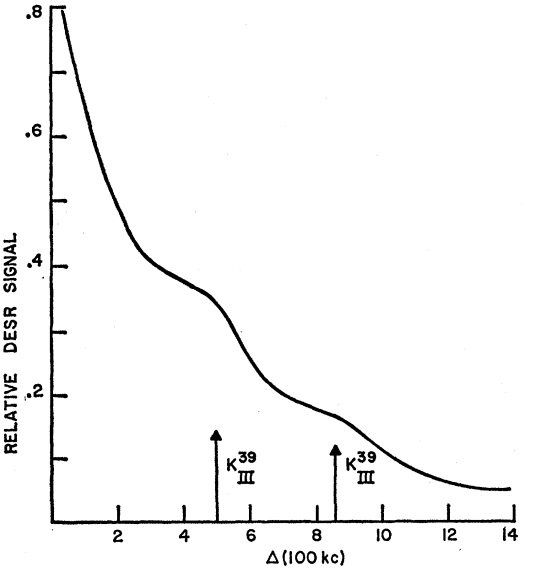

FIG. 13. DESR signal for $P=-27$ dB showing the K^{39} shell-III forbidden transition structure.

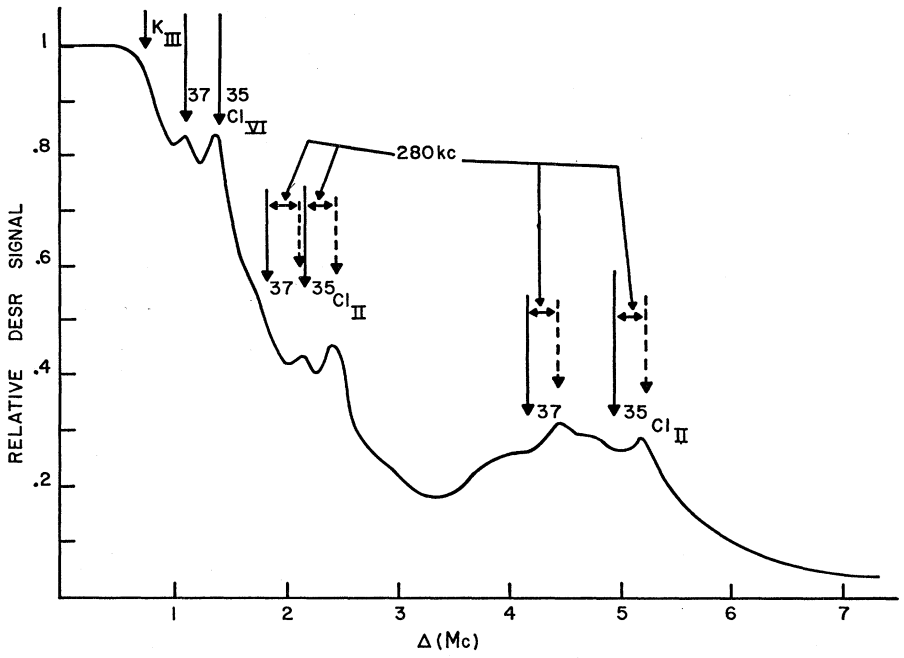

FIG. 14. DESR signal for $P=-6$ dB showing the forbidden transition structure.

ing to the shell-III K^{39} nuclei forbidden transitions are shown to be in agreement with the two bumps which appear in the experimental DESR signals.

The data in Fig. 14 were taken at a much higher pump level than that of Fig. 13 and the solid arrows shown at the larger values of Δ indicate the frequencies given in Table I for the shell-II Cl^{35} and Cl^{37} nuclei. One may note that if each of the predicted frequencies for shell II is shifted to a larger value of Δ by about 280 kc, then the resulting points, indicated by the dashed arrows in Fig. 14, fall upon resolved structure observed in the data. No explanation for this 280-kc shift has, as yet, been found.

Nuclear Relaxation

The semiquantitative agreement noted above between the experimental results and theoretical predictions for the forbidden transition intensity of the chlorine nuclei from the shell VI and more distant lattice sites were achieved by assuming a "zero" *nuclear* relaxation time. Appendix IIB outlines a calculation of the forbidden transition behavior for a system of spin-$\frac{1}{2}$ nuclei which have a finite *nuclear* reorientation rate, $\omega_n \equiv 1/T_n$. Although both K and Cl nuclei are spin-$\frac{3}{2}$, rather than the more simple spin-$\frac{1}{2}$ nuclei treated in Appendix IIB, the latter case is sufficient to give one a satisfactory qualitative picture of the system's behavior for nonzero nuclear reorientation times. In Appendix IIIB the important assumption is made that the *electron* does not relax via a forbidden transition with the nuclear-spin-level system under consideration. This is expected to be a valid assumption for the (211) nuclei in regard to which the most important conclusions are drawn.

The expression for the magnetization induced by the forbidden transitions with N nuclei in approximately equivalent positions about the F center is given in Eq. (II23) of Appendix II. An examination of the form of Eq. (II23) shows that the criterion for a "short" nuclear reorientation time is

$$N\omega_n \gtrsim \omega_1, \tag{3.32}$$

in which case the $(\omega_1/N\omega_n)$ term may be neglected in the denominator of Eq. (II23). This is then equivalent to the relation given in Eq. (II6) and the forbidden transitions saturate in the same manner as the allowed transitions, i.e., determined by the electronic relaxation rates only. On the other hand, if $N\omega_n < \omega_1$ then, from the form of Eq. (II23), it can be seen that the forbidden transitions would saturate more quickly and that the saturation point would be determined by a *nuclear* relaxation time.

Since the breadth of the central maxima in Fig. 12 indicate the importance of the shell-VI chlorines, the agreement of intensities noted earlier implies that these nuclei have a "fast" ω_n in the sense defined in Eq. (3.32), or that

$$\omega_n(211) \gtrsim (\omega_1/24) \approx 1.5\times 10^3 \text{ sec}^{-1}, \tag{3.33}$$

from the previous determination of the electron ω_1 given in Eq. (3.31).

This value of ω_n for the (211) Cl nuclei seems surprisingly large. It would not seem likely that this could arise via the usual dipolar mutual spin-flip processes against the bulk of the Cl nuclei since the (211) nuclei are split from the Zeeman frequency by at least 50 kc. Neither can one appeal to spin flips among the members of the

shell-VI group since this leaves the net nuclear polarization for these forbidden transitions unchanged.

An extremely important consequence of the inequality (3.33) is that the hyperfine interaction *cannot* be considered static as has been done in previous models for describing the steady state ESR behavior as well as in calculating the DESR response of the T_1-T_2 model in this paper.

IV. SUMMARY

The DESR techniques described in this paper can be successfully applied to the inhomogeneously broadened resonance line of F centers in KCl to gain information concerning the details of the absorption mechanisms which cannot be obtained in the usual single-frequency (ESR) experiment. The relative DESR signals predicted for the T_1-T_2 spin-packet model, which has formed the basis of previous treatments of the ESR behavior for the F-center system, are found to be inconsistent with the experimental results.

However, a general relation, which is independent of the specific model chosen to represent the system's response, is obtained to express the area under the DESR curves in terms of the intensity of the corresponding ESR absorption. The application of this relation to the data obtained in the experiment gives a KCl F-center spin-relaxation time at room temperature of $T_1=0.3\times10^{-4}$ sec with an estimated uncertainty of about 15%.

Much of the structure which is observed in the DESR curves can be unambiguously associated with "forbidden" transitions in which the F-center electron and a neighboring nucleus undergo a simultaneous spin flip. The calculated positions of the structure corresponding to the chlorine nuclei of shell II are found, however, to be uniformly shifted by about 280 kc from the peaks which are experimentally observed. Neither the origin of this shift nor the details of the shape of the associated structure for this particular group of nuclei is presently understood.

Even a conservative estimate of the total intensity associated with the observed forbidden transition structure indicates that, for moderately high applied-rf-field levels, these processes contribute at least 30% of the entire absorption signal. Their presence, therefore, accounts for a significant portion of the observed ESR absorption signal when the applied field, H_1, is somewhat larger than the saturation value, $H_{1/2}$. If it were not for this mechanism, the ESR saturation plot "droop" which was previously observed[1,3] and which motivated the DESR experiment would be more pronounced and would have been observed at smaller values of H_1.

The large intensity associated with the forbidden transitions of the 24 Cl nuclei of shell VI is shown to imply that the *nuclear* relaxation rate at these sites is sufficiently large that the hyperfine interaction cannot be treated as a static phenomenon. Changes in the local field at the F-center site due to the reorientation of one of these nuclei occur in a time which is at least as short as the electron T_1. Such local field fluctuations will, therefore, contribute to the packet broadening and in addition, one would expect to observe spectral diffusion effects as the "saturated" spins jump about in the inhomogeneous distribution, perhaps many times, before relaxing to the lattice.

These observations require that a new approach be taken for the proper description of the system. This problem is to be treated in a subsequent paper.

ACKNOWLEDGMENTS

The author wishes to thank Professor R. H. Silsbee, who directed the thesis upon which this paper is based, for the profit which he has derived from their frequent discussions. In addition, Professor Silsbee offered many invaluable specific suggestions among which, for example, were the suggestions that the techniques of degenerate perturbation theory could be applied to the problem of guide-to-guide coupling in the bimodal sample cavity, that a fundamental relation must exist between the DESR signal area and the corresponding pump absorption signal, and that the large intensity observed for the shell-VI Cl forbidden transitions must imply an unexpectedly fast nuclear relaxation time.

Special acknowledgment must also be given to Professor C. P. Slichter for his helpful comments during the preparation of this manuscript and particularly for pointing out to the author an invalid assumption in the original derivations of the second part of Appendix I and suggesting an approach which eliminated this error.

APPENDIX I: RELATION OF DESR SIGNAL AREA TO THE ESR ABSORPTION INTENSITY

A. Longitudinal Magnetization Induced by the Pump Fields

The purpose of this section is to show that the area under the DESR signal is directly proportional to the change in the z component of magnetization caused by the pump fields and, therefore, that the contribution to $S(P,\Delta)$ from the "rotary saturation" terms, $S_\beta(P,\Delta)$ has zero area as a function of Δ.

The spin-system Hamiltonian is written as

$$\mathcal{H}=\mathcal{H}_0+\mathcal{H}_P+\mathcal{H}_D\,, \tag{I1a}$$

where the pump interaction is

$$\mathcal{H}_P=\tfrac{1}{2}iP\textstyle\sum_j(S_j^+e^{ipt}-S_j^-e^{-ipt})\,, \tag{I1b}$$

the detector contribution is

$$\mathcal{H}_D=\tfrac{1}{2}iD\textstyle\sum_j(S_j^+e^{idt}-S_j^-e^{-idt})\,, \tag{I1c}$$

and all other interactions are included in $\mathcal{H}_0$. The density matrix elements are written as the sum of the thermal equilibrium component ρ_0, a component

induced by the pump fields ρ_P, and the detector component ρ_D. It is assumed that the detector field is sufficiently small that the system's response is linear in D and, therefore, that ρ_D is of order D.

Consider the interaction representation in which an operator Q is transformed into Q' by

$$Q'=\exp\left[i\int_0^t(\mathcal{H}_0+\mathcal{H}_P)d\tau\right]Q \times\exp\left[-i\int_0^t(\mathcal{H}_0+\mathcal{H}_P)d\tau\right]. \quad (I2)$$

The approximate solution for $\rho_D'(t)$ is given by

$$\rho_D'(t)=-i\int_{-\infty}^0[\mathcal{H}_D'(t+\tau),\rho_0'(t+\tau)+\rho_P'(t+\tau)]d\tau$$
$$=\tfrac{1}{2}D\int_{-\infty}^0(\textstyle\sum_j[S_j^{+\prime}\ t+\tau),\rho_0'(t+\tau)+\rho_P'(t+\tau)]$$
$$\times e^{id(t+\tau)}-\textstyle\sum_j[S_j^{-\prime}(t+\tau),\rho_0'(t+\tau),$$
$$+\rho_P'(t+\tau)]e^{-id(t+\tau)})d\tau. \quad (I3)$$

The detector absorption, $W_D(P,\Delta)$, under steady-state conditions is, as previously noted, given by

$$W_D(P,\Delta)=\tfrac{1}{2}dD\ \mathrm{Tr}\{\rho_D\textstyle\sum_j(S_j^+e^{idt}+S_j^-e^{-idt})\}_{\mathrm{d.c.}}$$
$$=\tfrac{1}{2}dD\ \mathrm{Tr}\{\rho_D'(t)\textstyle\sum_j(S_j^{+\prime}(t)e^{idt}$$
$$+S_j^{-\prime}(t)e^{-idt})\}_{\mathrm{d.c.}} \quad (I4)$$

which, using (I3), may be written

$$W_D(P,\Delta)$$
$$=\textstyle\sum_{jk}\frac{1}{4}dD^2\Big\{\int_{-\infty}^0\mathrm{Tr}(S_k^{-\prime}(t)[S_j^{+\prime}(t+\tau),$$
$$\rho_0'(t+\tau)+\rho_P'(t+\tau)]e^{id\tau})d\tau-\int_{-\infty}\mathrm{Tr}(S_k^{+\prime}(t)$$
$$\times[S_j^{-\prime}(t+\tau),\rho_0'(t+\tau)+\rho_P'(t+\tau)]e^{-id\tau})d\tau\Big\}. \quad (I5)$$

By expressing the elements in the second integral on the right-hand side of (I5) in terms of their Hermitian conjugates one may rewrite (I5) as

$$W_D(P,\Delta)=\textstyle\sum_{jk}\frac{1}{4}dD^2\int_{-\infty}^\infty\mathrm{Tr}\{S_k^{-\prime}(t)[S_j^{+\prime}(t+\tau),$$
$$\rho_0'(t+\tau)+\rho_P'(t+\tau)]\}e^{id\tau}d\tau. \quad (I5a)$$

Noting that the integrand in (I5a) may be identified with the Fourier transform, $\tilde{W}_D(P,\tau)$, of $W_D(P,\Delta)$ one may use the relation $\int_{-\infty}^\infty W_D(P,\Delta)d\Delta=2\pi\tilde{W}_D(P,0)$ to obtain

$$\int_{-\infty}^\infty W_D(P,\Delta)d\Delta$$
$$=\textstyle\sum_{jk}\frac{1}{2}dD^2\pi\ \mathrm{Tr}\{S_k^{-\prime}(t)[S_j^{+\prime}(t),\rho_0'(t)+\rho_P'(t)]\}$$
$$=\textstyle\sum_{jk}\frac{1}{2}dD^2\pi\ \mathrm{Tr}\{S_k^-[S_j^+,\rho_0+\rho_P]\}, \quad (I6a)$$

which, using the identity $\mathrm{Tr}\{A[\mathrm{B},C]\}=\mathrm{Tr}\{C[A,\mathrm{B}]\}$, may be rewritten as

$$\int_{-\infty}^\infty W_D(P,\Delta)d\Delta=dD^2\pi\textstyle\sum_j\mathrm{Tr}\{S_{zj}(\rho_0+\rho_P)\}, \quad (I6b)$$

where ρ_P is the steady-state value of $\rho_P(t)$. With no pump field applied $\rho_P=0$ and one obtains

$$\int_{-\infty}^\infty W_D(0,\Delta)d\Delta=dD^2\pi\textstyle\sum_j\mathrm{Tr}\{S_{zj}\rho_0\}. \quad (I6c)$$

Equation (I6c) is the usual expression for the area under an unsaturated absorption line so that if $g(d)$ is the normalized line shape of the absorption, one may write

$$W_D(0,\Delta)=dD^2\pi\textstyle\sum_j\mathrm{Tr}\{S_{zj}\rho_0\}g(p+\Delta), \quad (I7)$$

where $\sum_j\mathrm{Tr}\{S_{zj}\rho_0\}g(p+\Delta)$ is the thermal equilibrium magnetization per unit frequency at the detector frequency $(p+\Delta)$. At the pump frequency one may define

$$\textstyle\sum_j\mathrm{Tr}(S_{zj}\rho_0)g(p)\equiv\frac{1}{2}M_0, \quad (I8)$$

in the notation of the previous sections, which can be used to find

$$W_D(0,0)=dD^2\pi\tfrac{1}{2}M_0, \quad (I9)$$

and, therefore, from (I6b), (I6c), and (I9) one may write

$$\int_{-\infty}^\infty\frac{W_D(0,\Delta)-W_D(P,\Delta)}{W_D(0,0)}d\Delta$$
$$=\int_{-\infty}^\infty S(P,\Delta)d\Delta=-(\tfrac{1}{2}M_0)^{-1}\mathrm{Tr}\{\textstyle\sum_j S_{zj}\rho_P\}. \quad (I10)$$

Thus it is found that the integral of $S(P,\Delta)$, which may be written as the sum of the saturation component $S_\alpha(P,\Delta)$ and the rotary saturation component $S_\beta(P,\Delta)$, is related only to the M_z induced by the pump field. This relation as expressed in Eq. (I10), indicates that $\int_{-\infty}^\infty S_\beta(P,\Delta)d\Delta=0$ in general, the right-hand side of (I10) being just the result obtained for $\int_{-\infty}^\infty S_\alpha(P,\Delta)d\Delta$ alone since the term $\mathrm{Tr}\{\sum_j S_{zj}\rho_P\}$ is just the z component of magnetization induced by the pump fields, i.e., $\int\alpha(H)dH$ in the notation of Sec. III.

B. Relation of $\mathrm{Tr}(\sum_j S_{zj}\rho_P)$ to the Pump ESR Absorption

The purpose of this section is to indicate how $\mathrm{Tr}\{\sum_j S_{zj}\rho_P\}$ is related to the power absorbed from the pump fields and thereby demonstrate the relation between the area under the DESR signal, which Eq. (I10) shows to be proportional to $\mathrm{Tr}\{\sum_j S_{zj}\rho_P\}$, and the pump absorption.

Consider the response of the spin system with only the pump field applied. Under steady-state conditions, the time rate of change of M_z will be zero so that one may write

$$0=\mathrm{Tr}\{\textstyle\sum_j S_{zj}\dot{\rho}\}=\mathrm{Tr}\{\sum_j S_{zj}[-i\mathcal{H}_0,\rho]\}+\mathrm{Tr}\{\sum_j S_{zj}[-i\mathcal{H}_P,\rho]\}, \quad \text{(I11)}$$

where ρ is the steady-state density matrix and, as before, $\mathcal{H}_0$ includes all the interactions of the system, e.g., Zeeman interaction with the static field, nuclear-nuclear dipolar terms, electron-electron dipolar terms, hyperfine interactions, spin-lattice terms, etc., except the rf interaction with the pump field which is included as the $\mathcal{H}_P$ term in (I11). If one writes $\rho=\rho_0+\rho_P$, as in Sec. A, then from the special case when $\mathcal{H}_P=0$ and $\rho_P=0$ one sees that $[\mathcal{H}_0,\rho_0]=0$. In addition, one may write

$$\mathrm{Tr}(\textstyle\sum_j S_{zj}[-i\mathcal{H}_P,\rho])=\mathrm{Tr}(\sum_j \rho[S_{zj},-i\mathcal{H}_P])=\tfrac{1}{2}P\,\mathrm{Tr}\{\sum_j \rho(S_j^+e^{ipt}+S_j^-e^{-ipt})\}, \quad \text{(I12a)}$$

where the trace in the final expression of (I12a) is just the expectation value of electron-spin transverse magnetization rotating about H_0 at a frequency p. Since this is zero for the thermal-equilibrium case, one may take

$$\mathrm{Tr}(\textstyle\sum_j S_{zj}[-i\mathcal{H}_P,\rho_0+\rho_P])=\mathrm{Tr}(\sum_j S_{zj}[-i\mathcal{H}_P,\rho_P]), \quad \text{(I12b)}$$

and write (I11) as

$$\mathrm{Tr}(\textstyle\sum_j S_{zj}\dot{\rho}_P)_{ss}=\mathrm{Tr}(\sum_j S_{zj}[-i\mathcal{H}_0,\rho_P])_{ss}+\mathrm{Tr}(\sum_j S_{zj}[-i\mathcal{H}_P,\rho_P])_{ss}. \quad \text{(I13)}$$

In addition, the second trace on the right of (I13) may be written as

$$\mathrm{Tr}(\textstyle\sum_j S_{zj}[-i\mathcal{H}_P,\rho_P])_{ss}=\mathrm{Tr}(\rho_P\sum_j[S_{zj},-i\mathcal{H}_P])_{ss}=\mathrm{Tr}(\rho_P(1/\dot{p})\mathbf{M}\cdot d\mathbf{P}(t)/dt)_{ss}=P(P\chi''(\mathrm{pump};P)), \quad \text{(I14)}$$

so that one may express (I13) in the form

$$\mathrm{Tr}(\textstyle\sum_j S_{zj}\dot{\rho}_P)_{ss}=\mathrm{Tr}(\sum_j S_{zj}[-i\mathcal{H}_0,\rho_P])_{ss}+P(P\chi''(\mathrm{pump};P)). \quad \text{(I15)}$$

Consider now the first term on the right of (I15) which may be written as $\mathrm{Tr}(\sum_j \rho_P[S_{zj},-i\mathcal{H}_0])$. The only terms in $\mathcal{H}_0$ which do not commute with S_z are the S_x and S_y parts of spin-lattice interaction, $\mathcal{H}_{SL}^{\pm}(t)$ and those parts of the hyperfine interaction involving S_x or S_y. However, these matrix elements of the hyperfine interaction which enter in computing the trace of $(\sum_j S_{zj}[-i\mathcal{H}_0,\rho_P])$ give time-dependent terms which oscillate at about the electron Larmor frequency and consequently do not contribute to the steady-state values which one observes averaged over some period of time appropriate to the response characteristics of the measuring apparatus. Thus Eq. (I15) is written

$$0=\mathrm{Tr}(\textstyle\sum_j S_{zj}\dot{\rho}_P)_{ss}=\mathrm{Tr}(\sum_j S_{zj}[-i\mathcal{H}_{SL}^{\pm}(t),\rho_P])_{ss}+P(P\chi''), \quad \text{(I15b)}$$

which is only the statement that, under steady-state conditions, the net rate of rf-induced spin transitions is just equal to the net rate of spin-lattice transitions. The interaction term, $\mathcal{H}_{SL}^{\pm}(t)$, which describes this latter process is taken to be of the form

$$\mathcal{H}_{SL}^{\pm}(t)=\textstyle\sum_j[A_j(t)S_{xj}+B_j(t)S_{yj}], \quad \text{(I16a)}$$

where for example, if the spin-lattice coupling arises from a modulation of the hyperfine interaction, $A(t)$ and $B(t)$ may be defined as

$$A(t)=a(t)(\mathbf{I}\cdot\mathbf{X}), \quad \text{(I16b)}$$

and

$$B(t)=b(t)(\mathbf{I}\cdot\mathbf{Y}). \quad \text{(I16c)}$$

In (I16b) and (I16c) $\mathbf{I}$ is the nuclear-spin operator and $\mathbf{X}$ and $\mathbf{Y}$ are, respectively, the electron-spin x and y components of the hyperfine-modulation tensor. In any case, the short correlation time which characterizes the spin-phonon interaction insures that the only significant contributions[21] to the relaxation process come from terms quadratic in $\mathcal{H}_{SL}$. One may then show in a straightforward fashion that the first term on the right of Eq. (I15b) is validly approximated as

$$\mathrm{Tr}(\textstyle\sum_j S_{zj}[-i\mathcal{H}_{SL}^{\pm}(t),\rho_P])=-\mathrm{Tr}\left(\rho_P\sum_j\int_{-\infty}^{\infty}\tfrac{1}{2}e^{i\omega_j t}\times\{A_j(t)A_j(t+t')+B_j(t)B_j(t+t')\}dt'S_{zj}\right), \quad \text{(I17)}$$

where ω_j is the resonant frequency of the jth electron. The integral in (I17) may be defined as

$$\int_{-\infty}^{\infty}\tfrac{1}{2}e^{i\omega_j t'}\{A_j(t)A_j(t+t')+B_j(t)B_j(t+t')\}\equiv\omega_{1j}, \quad \text{(I18a)}$$

so that

$$\mathrm{Tr}(\textstyle\sum_j S_{zj}[-i\mathcal{H}_{SL}^{\pm},\rho_P])=-\mathrm{Tr}(\sum_j\omega_{1j}\rho_P S_{zj}). \quad \text{(I18b)}$$

[21] These points are discussed in Chap. VIII of Ref. 12 and in Chap. 5 of *Principles of Magnetic Resonance* by C. P. Slichter (Harper and Row, New York, 1963).

It should be noted that there is no obvious justification that ω_{1j} may be treated merely as a number and factored from the sum over the states associated with the jth electron. For example, in the case of spin-lattice relaxation by hyperfine modulation the A and B terms which enter in the definition of ω_{1j} in (I18a) are functions of nuclear-spin operators and may therefore depend upon the distribution in the nuclear states. This distribution may, in turn, depend in detail upon the rf interaction because of such processes as the "forbidden" transitions and consequent dynamic nuclear polarization. However, if the spin-lattice coupling does *not* involve nuclear operators, or if it does involve nuclear operators, but in a manner such that $A^2(t)$ and $B^2(t)$, as defined in Eqs. (I16b) and (I16c), are not sensitive to the specific nuclear state, or if the nuclear state distributions are essentially uneffected by the rf interaction over the range of P in which one is interested and if the spectral distribution of $A(t)$ and $B(t)$ is practically uniform over the range of the electron resonant frequencies, then an average relaxation rate, ω_1, which is independent of P may be defined by

$$\omega_1 \equiv \mathrm{Tr}(\textstyle\sum_j \omega_{1j}\rho_P S_{zj})\{\mathrm{Tr}(\sum_j \rho_P S_{zj})\}^{-1}. \quad \text{(I19)}$$

In such a case, Eq. (I15b) may be written as

$$0=\mathrm{Tr}(\textstyle\sum_j S_{zj}\dot{\rho}_P)_{ss}=-\omega_1\,\mathrm{Tr}(\sum_j \rho_P S_{zj}) + P[P\chi''(\mathrm{pump};P)], \quad \text{(I20)}$$

which may be substituted in Eq. (I10) to obtain

$$\int_{-\infty}^{\infty} S(P,\Delta)d\Delta=(\tfrac{1}{2}M_0\omega_1)^{-1}P[P\chi''(\mathrm{pump};P)], \quad \text{(I21)}$$

as stated in Eq. (3.29).

APPENDIX II: FORBIDDEN TRANSITION INTENSITIES

A. Shell VI Cl^{35} Nuclei When Components Are Unresolved

General approach. In this Appendix the equations are expressed in the same units as were introduced in Sec. III, i.e., $\hbar=1$ and magnetic field units as defined in Eq. (3.2). Figure 15 illustrates the energy-level system of an electron coupled to a single spin-$\frac{3}{2}$ nucleus. The hyperfine splittings indicated in Fig. 15 include only the dominant isotropic hyperfine term a.

The dotted arrow in Fig. 15 shows one of the forbidden transitions which occurs at a frequency $H_0-a-\gamma_I H_0$, where γ_I is the gyromagnetic ratio of the nucleus relative to that of the electron. This forbidden transition tends to saturate two different allowed transitions since it removes a spin from the ground state of the allowed transition of energy $(H_0-3a/2)$ and places a spin in the excited state of the allowed transition of energy $(H_0-a/2)$. The forbidden saturation components, therefore, occur at frequencies which

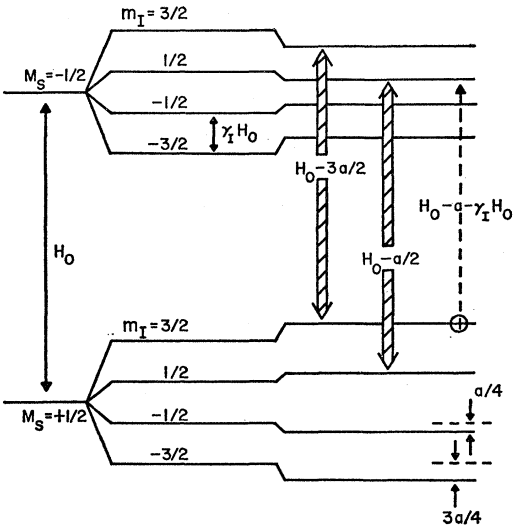

FIG. 15. Level diagram for an electron coupled to a single $I=\frac{3}{2}$ nucleus with hyperfine coupling a. γ_I is the relative gyromagnetic ratio of the nucleus.

differ from the applied radio frequency by $(\gamma_I H_0+a/2)$ and $(\gamma_I H_0-a/2)$.

The calculations in this part of Appendix II are carried out for the total forbidden transition intensity assuming that the hyperfine coupling is sufficiently small that the two components are unresolved and assuming a "fast" nuclear relaxation rate. Calculations for resolved components and a finite nuclear relaxation rate are carried out in part B.

The system is treated using the T_1-T_2 model discussed in Sec. 3 and a comparison of the results of this Appendix with the experimental data may be made by finding the area under the predicted forbidden transition curves since, by a simple extension of the general relation derived in Appendix I, this area depends only on the pump power absorbed in these transitions and the electron T_1.

The hyperfine-interaction Hamiltonian may be written as

$$\mathcal{H}_{\mathrm{hfs}}=\mathbf{S}\cdot(\mathbf{A}+\mathbf{B})\cdot\mathbf{I}, \quad \text{(II1)}$$

where $\mathbf{A}$ and $\mathbf{B}$ are, respectively, the isotropic and anisotropic components of the hyperfine tensor. If the hyperfine fields at the electron are small compared with the static field H_0, the hyperfine energy may be approximated as

$$\omega_{\mathrm{hfs}}=M_S a I_z+M_S B_{zz}I_z+M_S B_{zx}I_x + M_S B_{zy}I_y \equiv \gamma_I \mathbf{H}_{ei}\cdot\mathbf{I}, \quad \text{(II2)}$$

where $\mathbf{H}_{ei}$ is interpreted as the local magnetic field produced by the electron at the site of the nucleus. The Hamiltonian term in (II1) may then be included in the equations of motion for the density matrix elements. These equations are next solved to find the steady-state diagonal element, α_f, corresponding to the longitudinal

magnetization induced by forbidden transitions. For the case of a single nucleus one obtains

$$0=\frac{-P^2\omega_2(\frac{1}{2}M_0+\alpha_a+\alpha_f)|\langle m_I'|e^{(\phi/2)(I_+-I_-)}|m_I\rangle|^2}{\omega_2^2+(H\pm\gamma_I H_0)^2}-\omega_1\alpha_f, \quad \text{(II3)}$$

where α_a is the allowed transition magnetization, $m_I'\neq m_I$, and the states $|m_I\rangle$ are nuclear spin states with z component of spin quantum number m_I. The angle ϕ, which appears in the spin rotation operator, $e^{(\phi/2)(I_+-I_-)}$, of Eq. (II4), is defined by:

$$\phi\equiv\text{the angle between } [(H_0\hat{z}+\mathbf{H}_{ei}) \text{ with } m_S=+\tfrac{1}{2}] \text{ and } [(H_0\hat{z}+\mathbf{H}_{ei}) \text{ with } m_S=-\tfrac{1}{2}]. \quad \text{(II4)}$$

The other quantities used in Eq. (II3) are the same as previously defined in Sec. III. A more detailed derivation for transition probabilities in an analogous problem of simultaneous electron-nucleus spin flips can be found in the paper of Trammel, Zeldes, and Livingston.[15]

If there are several nuclei contributing to the forbidden transition intensity at the same frequency then the contribution from the kth nucleus, $\alpha_{f;k}$, may be obtained from Eq. (II3) if one replaces α_a by the term $(\alpha_a+\sum_{j\neq k}\alpha_{f;j})$. One then finds

$$0=\frac{-P^2\omega_2}{\omega_2^2+(H\pm\gamma_I H_0)^2}[\tfrac{1}{2}M_0+(\alpha_a+\sum_{j\neq k}\alpha_{f;j})+\alpha_{f;k}]\times|\langle m_I'|R_k|m_I\rangle|^2-\omega_1\alpha_{f;k}, \quad \text{(II5)}$$

where $R_k=e^{(\phi_k/2)(I_+k-I_-k)}$. If Eq. (II5) is summed over all contributing nuclei, with $\sum\alpha_{f;k}\equiv\alpha_f$, one obtains

$$\alpha_f=\frac{-P^2(\omega_2/\omega_1)(\frac{1}{2}M_0+\alpha_a)[\sum|\langle m_I'|R_k|m_I\rangle|^2]}{\omega_2^2+P^2(\omega_2/\omega_1)[\sum|\langle m_I'|R_k|m_I\rangle|^2]+(H\pm\gamma_I H_0)^2}. \quad \text{(II6)}$$

The expression for α_f given in Eq. (II6) may then be used in the DESR signal area relation given in Appendix I, Eq. (I10) if one wishes to compare these results with the experimental data.

Intensity from shell-VI and more distant Cl nuclei. The Cl nuclei of shell VI are located in [211] directions from the F center and have an isotropic hyperfine coupling of 100 kc. This may be neglected in relation to the static field (1.4 Mc) in calculating the angle ϕ. The change in transverse field, $\delta(H_{ei})_x$,

$$[\gamma_I\delta(H_{ei})_x]_{211}=3b\cos\theta\sin\theta=3(5/36)^{1/2}b\approx b, \quad \text{(II7)}$$

and

$$[\gamma_I\delta(H_{ei})_x]_{112}=3b(8/36)^{1/2}\approx 1.4b, \quad \text{(II8)}$$

for any (211) nuclei. ENDOR measurements[18–20] give the Cl^{35} anisotropic term, b, as about 30 kc for the shell-VI nuclei in KCl. Thus, the angle ϕ is approximately

$$\phi(\text{KCl } 211)=2\times10^{-2}, \quad \text{(II9)}$$

and

$$\phi(\text{KCl } 112)=2.8\times10^{-2}. \quad \text{(II10)}$$

The rotation operator is then approximated as

$$R=\exp(\tfrac{1}{2}\phi(I_+-I_-))\simeq 1+\tfrac{1}{2}\phi(I_+-I_-)\simeq\begin{cases}[1+(10^{-2})(I_+-I_-)] & \text{for (211)Cl}\\ [1+(1.4\times10^{-2})(I_+-I_-)] & \text{for (112)Cl.}\end{cases} \quad \text{(II11)}$$

For the forbidden transition occurring at a larger frequency than the corresponding allowed transition only the I_- term enters and one finds

$$|\langle m_I-1|R|m_I\rangle|^2_{(211)}=10^{-4}[I(I+1)-m_I(m_I-1)], \quad \text{(II12a)}$$

and

$$|\langle m_I-1|R|m_I\rangle|^2_{(112)}=2\times10^{-4}[I(I+1)-m_I(m_I-1)], \quad \text{(II12b)}$$

where at room temperature one may take $[I(I+1)-m_I(m_I-1)]$ to be its average value of 2.5. The sum over the contributing nuclei which appears in (II6) is, for the 24 shell-VI Cl ions,

$$\sum_{\text{shell VI}}|\langle m_I-1|R|m_I\rangle|^2=16(2.5\times10^{-4})+8(2.5\times2\times10^{-4})=8\times10^{-3}. \quad \text{(II13)}$$

Since no ENDOR data are available for those Cl nuclei farther from the F center than shell VI, it is necessary to estimate the magnitudes of the anisotropic fields from the ordinary dipolar expression. If one calculates the anisotropic fields due to the classical dipolar terms for the shell-VI sites, assuming the electron to be localized in the center of the anion vacancy, one finds that the values so obtained are only about 25% different from the measured values. This implies that there is little remaining electron-wavefunction gradient, which gives large local contributions to the expectation value of terms of the form $[zx(r)^{-5}]$, at the shell-VI sites. This observation may be used to justify the localized F-center approximation in the following calculations for Cl nuclei which are even farther from the F center than those of shell VI.

In the localized electron approximation one finds the anisotropic terms of the hyperfine tensor to be

$$B_{zx}=3xz(r)^{-5}, \quad \text{(II14)}$$

where x, z, and r are taken as the appropriate distances from the nucleus to the center of the anion vacancy. The 12 shell-VIII Cl nuclei located at (200) positions are found to have, using (II14), (II2), and the KCl lattice constant of 3.14 Å, a total contribution

$$\sum_{\text{shell VIII}}|\langle m_I-1|R|m_I\rangle|^2\approx10^{-3}. \quad \text{(II15)}$$

The next Cl shell (X) is found at 10 Å from the F center. The contribution to the forbidden transition probability from this shell and from all shells farther away is estimated by assuming an essentially uniform spherical distribution of Cl sites and performing an integration over the volume extending from shell X to infinity. The result is

$$\int_{\text{shell X}}^{\infty} |\langle m_I-1|R|m_I\rangle|^2 dv \approx 10^{-3}, \qquad \text{(II16)}$$

and therefore, the total expected intensity found near $\Delta=1.4$ Mc, which is obtained by using the sum of Eqs. (II16), (II15), and (II13) in the expression for α_f of (II6), is

$$\alpha_f=\frac{-P^2(\omega_2/\omega_1)(\frac{1}{2}M_0+\alpha_a)(10^{-2})}{\omega_2{}^2+P^2(\omega_2/\omega_1)(10^{-2})+(H-\gamma_I H_0)^2}. \qquad \text{(II17)}$$

In order to compare the prediction of Eq. (II17) with the data in Fig. 12 one may determine the pump level at which the *allowed* transition area would be equal to the *forbidden* transition area obtained from (II17). The factor of 10^{-2} in (II17) represents a 20 dB decrease in intensity as compared with the predicted allowed transition intensity in Eq. (3.16a). The experimental results shown in Fig. 12 were taken at $P=-9$ dB and indicated an α_a of about $-\frac{1}{2}(\frac{1}{2}M_0)$. Thus, Eq. (II17) predicts an α_f at -9 dB equal to about one-half the α_a at -30 dB with the appropriate integrals, therefore giving the same factor of $\frac{1}{2}$ between the relative DESR areas, as stated in Sec. III.

B. Finite Nuclear Relaxation Rates and Resolved Components

Consider the case of an electron coupled to a single spin-$\frac{1}{2}$ nucleus, the energy-level diagram of which is shown in Fig. 16. To calculate the steady-state-induced longitudinal magnetization for this system one need only consider the diagonal elements of the density matrix which are proportional to the statistical occupation numbers n_i; $i=1, 2, 3, 4$. In this treatment it is assumed that the rf field is resonant *only* with the forbidden transition (1–4) and that its effect upon the forbidden transition (1–3) may be neglected. It is further assumed that the forbidden transition frequency is sufficiently far removed from the allowed transition frequencies that the effect of the allowed transition inducted magnetization may be approximated by an effective temperature which determines the relative occupations of levels 1 and 3 (or 2 and 4) in the absence of forbidden transitions. In this approximation the spin-lattice processes attempt to restore an occupation in, for example, level 1 of $(n_1)_0$;

$$(n_1)_0=(n_1+n_3)\tfrac{1}{2}(1+f_a), \qquad \text{(II18a)}$$

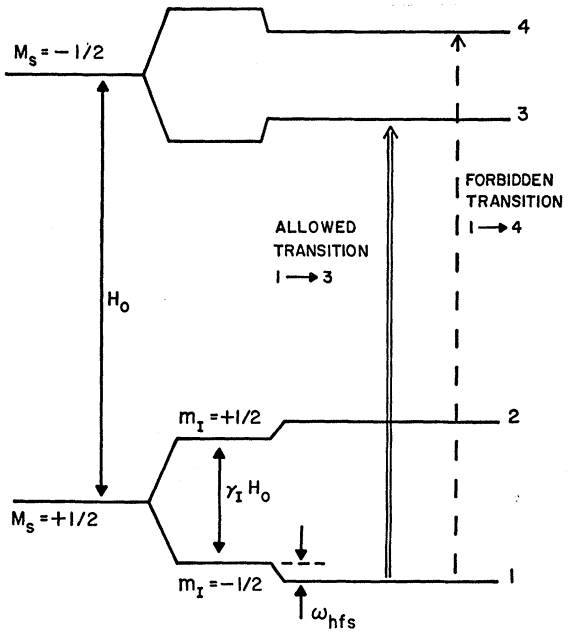

FIG. 16. Level diagram for an electron coupled to a single $I=\frac{1}{2}$ nucleus.

where f_a is a factor determined by the true lattice temperature and the allowed transition rate caused by the applied rf field. Another important assumption which is used in this treatment is the relaxation processes corresponding to "forbidden" relaxation, i.e., a spin-lattice transition between levels 1 and 4 (or between levels 2 and 3), may be neglected in comparison with "allowed" relaxation processes, i.e., between levels 1 and 3 (or 2 and 4). A nuclear relaxation rate ω_n is also assumed to exist which, for the nuclear splittings and temperatures appropriate to the experiment described in this paper, tends to equalize the populations of levels 3 and 4 (and the populations of 1 and 2).

The steady-state forbidden transition rate per unit magnetization found in (II3) is defined as

$$\frac{P^2\omega_2|\langle m_I'|R|m_I\rangle|^2}{\omega_2{}^2+(H\pm\gamma_I(H_0+H_{ei}))^2}\equiv R_f. \qquad \text{(II18b)}$$

Under the assumptions noted above the following set of equations for the steady-state occupation numbers is obtained:

$$-R_f(n_1-n_4)-\omega_1[n_1-\tfrac{1}{2}(1+f_a)(n_1+n_3)] -(\omega_n/2)(n_1-n_2)=0, \qquad \text{(II19a)}$$

$$-\omega_1[n_2-\tfrac{1}{2}(1+f_a)(n_2+n_4)] -(\omega_n/2)(n_2-n_1)=0, \qquad \text{(II19b)}$$

$$-\omega_1(n_3-\tfrac{1}{2}(1-f_a)(n_1+n_3)) -(\omega_n/2)(n_3-n_4)=0, \qquad \text{(II19c)}$$

and

$$n_1+n_2+n_3+n_4=2M, \qquad \text{(II19d)}$$

where $2M$ is the total number of electron-nucleus pairs. This set of equations may be solved to find the difference in population between the various levels;

$$(n_1-n_2)=-Mf_aR_f[\omega_n+\omega_1(1+f_a)]\times[\omega_n(\omega_1+\omega_n)J]^{-1}, \quad \text{(II20a)}$$

$$(n_3-n_4)=-Mf_aR_f[\omega_n+\omega_1(1-f_a)]\times[\omega_n(\omega_1+\omega_n)J]^{-1}, \quad \text{(II20b)}$$

$$(n_1-n_3)=Mf_a\{1+(R_f/\omega_n)\times[1-f_a(1+(\omega_n/\omega_1))^{-1}]\}J^{-1}, \quad \text{(II20c)}$$

$$(n_2-n_4)=Mf_a\{1+(R_f/\omega_n)\times[1+f_a(1+(\omega_n/\omega_1))^{-1}]\}J^{-1}, \quad \text{(II20d)}$$

where

$$J=1+(R_f/\omega_1)[1+(\omega_1/\omega_n)]. \quad \text{(II20e)}$$

One may note that, in the limit of large R_f and $\omega_n \ll \omega_1$, the nuclear level population differences given in Eqs. (II20a) and (II20b) obey the usual dynamic polarization relations.

One may subtract the allowed transition contribution, Mf_a, from the expressions given in (II20c) and (II20d) to find the forbidden transition contributions, $(n_1-n_3)_f$ and $(n_2-n_4)_f$,

$$(n_1-n_3)_f=-Mf_aR_f\{(1/\omega_1)+(f_a/\omega_n)\times[1+(\omega_n/\omega_1)]^{-1}\}J^{-1}, \quad \text{(II21a)}$$

$$(n_2-n_4)=-Mf_aR_f\{(1/\omega_1)-(f_a/\omega_n)\times[1+(\omega_n/\omega_1)]^{-1}\}J^{-1}. \quad \text{(II21b)}$$

First consider the situation in which one is concerned with the total intensity from both components, e.g., the unresolved components of the Cl shell VI and more distant Cl nuclei observed near 1.4 Mc. In this case

$$\delta n_f \equiv (n_1-n_3)_f+(n_2-n_4)_f=-2Mf_aR_f(\omega_1J)^{-1} \quad \text{(II22a)}$$

or, in the notation of Sec. III,

$$\alpha_f=-(\tfrac{1}{2}M_0+\alpha_a)R_f(\omega_1J)^{-1}. \quad \text{(II22b)}$$

Using the same procedure outlined in Eqs. (II5) and (II6) one may calculate, from the single nucleus expression in (II22), the total forbidden transition magnetization developed for the case of N equivalent contributing nuclei;

$$\alpha_f(\text{total})=\frac{-((\tfrac{1}{2}M_0)+\alpha_a)NR_f}{\omega_1+NR_f(1+(\omega_1/N\omega_n))}, \quad \text{(II23)}$$

which is used in justifying the "short" nuclear reorientation time criterion given in Eq. (3.32).

The factor f_a which appears in (II18a) is at most

$$f_a \approx (H_0/2kT) \approx 10^{-3} \text{ (at room temperature)}. \quad \text{(II24)}$$

Therefore, provided that $\omega_n \gg 10^{-3}\ \omega_1$, the terms $(f_a/\omega_n)[1+(\omega_n/\omega_1)]^{-1}$, which are found in (II21a) and (II21b), may be neglected in comparison with $(1/\omega_1)$. Under this condition, the expressions for $(n_1-n_3)_f$ and $(n_2-n_4)_f$ given in Eqs. (II21) are the same which justifies the statement of Sec. III that the two components of the shell-VI Cl forbidden transition intensity located at Δ's of (1.4−0.05) Mc and (1.4+0.05) Mc would be expected to have equal intensities.